

EVOLUTION OF COOLING LENGTH IN PARTS CREATED THROUGH LASER POWDER BED FUSION ADDITIVE MANUFACTURING

Zachary C. Reese¹, Jason Fox², John Taylor¹, and Chris Evans¹

¹ Center for Precision Metrology
University of North Carolina at Charlotte
Charlotte, North Carolina, USA

² The National Institute of Standards and Technology*
Gaithersburg, Maryland, USA

ABSTRACT

Additive manufactured (AM) components, specifically those created through laser powder bed fusion (LPBF) methods, exhibit an abundance of surface textures of varying forms and patterns. These topographies have historically been categorized solely using their R_a values, a metric which offers limited information to discern differences among the morphologies of AM surfaces. This diversity is illustrated not only among parts made using different machines or processing parameters, but also between different locations in the build chamber and even on the same part. Current instruments have the potential to acquire three dimensional (3D) maps of the AM surface, enabling a range of field and feature based descriptors that offer potential in characterizing AM surface morphology. This work explores feature-based metrology of AM surfaces in an effort to relate features to part quality, as well as aid the modeling community in better understanding of melt pool geometry. The feature of interest in this work, the chevron pattern seen on top of scan lines, is theorized to be connected to the laser parameters used in the printing of the part. This research explores the chevron pattern, observing changes in this feature over a range of laser power and velocity combinations.

INTRODUCTION

Metal AM is a growing technology which fabricates parts directly from 3D computer aided design (CAD) models. Parts are built up layer-by-layer starting at the substrate. A single layer of

metal powder is deposited over the substrate and the first layer of the part is selectively melted, fusing with the substrate. The build plate is lowered, and the process repeats until the part is completed. The layer-by-layer building of these parts allows for them to be created with complex geometries not attainable through traditional manufacturing methods.

Though AM processes can create geometries that other methods cannot, they are not without their own disadvantages. Parts often take on the order of hours to days being built and suffer from poor "as-printed" surface quality. While finishing processes such as laser ablation or bead blasting can improve surface roughness [1-4], the increasing complexity of these parts can render these processes ineffective. These rough surfaces are a major hurdle in the full-scale implementation of AM [5], as the understanding of their morphology is still in its adolescence. Often, these complex surfaces were being categorized by their R_a values alone; however, it has been shown that these classical parameters prove to be similar for visibly different surfaces [6-9]. In previous works, the authors have shown that based on the areal average roughness (S_a), as well as other parameters outlined in International Organization for Standards (ISO) 27178-2 [14], that it is impossible to discern between two qualitatively different surfaces (Figure 1) [6]. Additionally, two works by Fox *et al.* launched an investigation into downward facing, as-printed surfaces. These works

*Official contribution of the National Institute of Standards and Technology (NIST); not subject to copyright in the USA. The full descriptions of the procedures used in this paper require the identification of certain commercial products. The inclusion of such information should in no way be construed as indicating that such products are endorsed by NIST or are recommended by NIST or that they are necessarily the best materials, instruments, software, or suppliers for the purposes described.

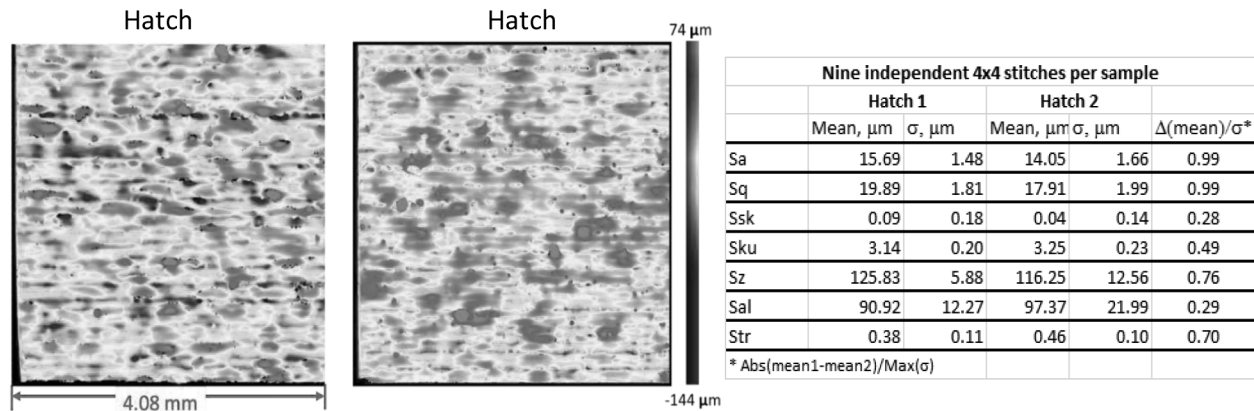


FIGURE 1. Comparison of two different metal AM surfaces based on ISO parameters

conclude that the use of R_a alone is insufficient in discerning the difference between surfaces predominantly covered by powdered metal particles and those dominated by scan tracks [7,8]. This has driven a push toward feature-based investigation for surface characterization. Rather, many researchers are beginning to rely on surface features to characterize metal AM parts [6-9].

With the previous standard method returning very little in the way of new surface information and a push toward feature-based investigation for surface characterization, the authors have identified the prominent chevron pattern that is often seen on upward facing surfaces of AM parts as a feature of interest (Figure 2). It is theorized that the chevron pattern may be linked to the dimensions of the melt pool.



Figure 2. Chevron pattern on upward facing surface of AM part

Preliminary work in numerical simulation has been performed in an effort to suitably model the melt pool dimensions for given build parameters. Gockel and Beuth have shown that, through finite element simulation, one can predict microstructure and grain morphology in Ti-6Al-4V. When operating in certain regions of the laser power-velocity (PV) process map, one can control the melt pool geometry and affect the cooling rate of single scan passes [10]. Other modeling attempts have explored this idea, for various nickel alloys rather than titanium. Keller *et al.* simulated the laser melt pool in nickel alloy 625 using finite element analysis. Simulations matched the surface temperatures captured in-situ with thermographic measurements in order to approximate thermal conditions beneath the surface of the scan line. Understanding these thermal conditions will allow one to predict and eventually control microstructure during builds [11]. This work was further expanded on by Ghosh *et al.* extending the same numerical simulations to nickel alloy 718 [12].

EXPERIMENTAL SETUP

The first step in this feature-based metrological approach was to look at the scan lines that appear on the top of the build without outside influence from the rest of the surface. To make this case as simple as possible, a number of single scans without powder were printed to build knowledge about the scan lines themselves. Single scans were printed into a nickel alloy 625 substrate in an EOS M270 Direct Metal Laser Sintering (DMLS) machine. These scan lines have a chevron pattern that occurs on the top of each line and is qualitatively different between scans of different PV combinations (Figure 3). Given this variation in the pattern, the angle

between the legs of the chevrons was chosen as a metric to quantify these variations.

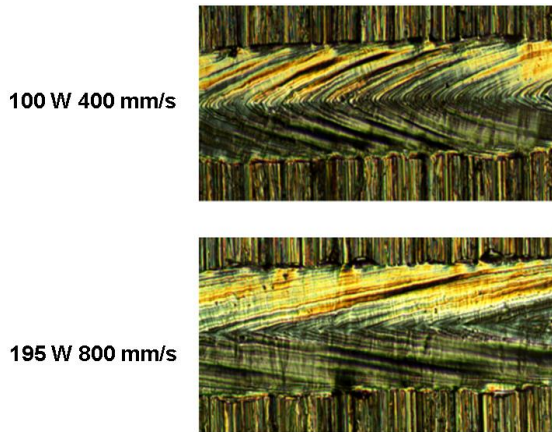


FIGURE 3. Variation in chevron pattern between different laser power and velocity combinations

If one knows the angle of this pattern and the width of the scan track, it is trivial to back out the length of the melt pool from its widest (and deepest) point to the tail. The length of the solidified melt pool from the tip of the chevron to the point where the legs reach the width of the scan line will be referred to as the “cooling length” (Figure 4). The importance of cooling length is described in another work by Gockel *et al.* who show that the cooling length is correlated with the microstructure of that track after cooling [12]. This information can potentially supplement the in-situ thermal data for validating models of melt pool dimension.

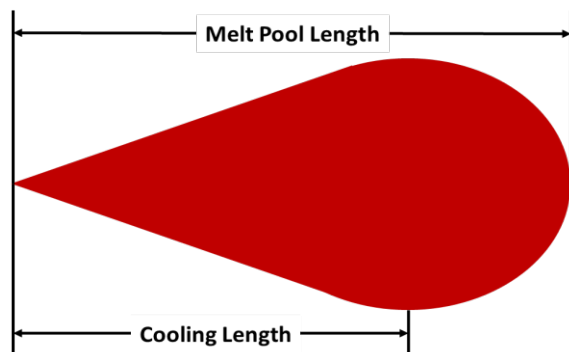


FIGURE 4. Distinction between melt pool length and cooling length

All builds for this paper were conducted in an EOS M270 DMLS machine. Six sets of 24 single pass scan tracks were printed over the course of two days to investigate the stability of this feature run to run as well as day to day. Each scan line is 10 mm long and offset by 2.5 mm from the

previous line. This ensures that the melt pool has sufficient time to reach steady state conditions in each line and is not influenced by the residual heat of the previous tracks. Power and velocity (PV) combinations are shown in Figure 5. Single scan lines ensure the chevron structure occurs in the middle of the track with little variation in the angle between the legs of each chevron. Printing with only beam on plate (i.e., no metal powder) mitigates any chance of spatter particles ejecting from the melt pool, denuding effects which can cause irregularity in the scan lines, partially melted powder particles adhering to the surface, and the variability of powder layer thickness.

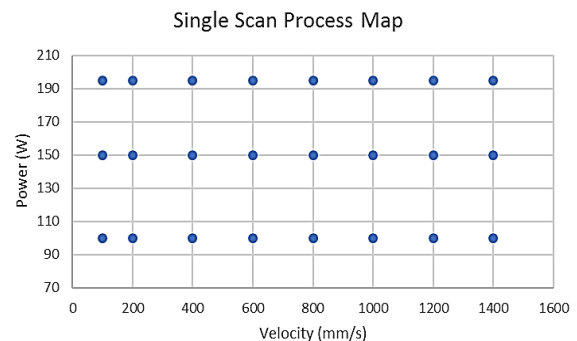


FIGURE 5. PV combinations for scan lines

Once printed, height maps of the single scans were obtained using a coherence scanning interferometer (CSI) and processed using a commercial software package. Each scan line was stitched with a 20x objective (418 μm^2 field of view (FOV)) with an overlap of 20 % between sites. After the data is leveled and the height data from the base plate removed, it can be seen in Figure 6A that the chevron pattern is barely visible in the unfiltered measurement. Even the larger spatial frequency chevrons are roughly an order of magnitude smaller than the scan line itself. Removing a best fit cylinder flattens the scan line, improving the visualization of the chevron pattern. The pattern can be further highlighted by applying appropriate Fourier filters. Figure 6B shows the same scan line with a Fourier band-pass filter at a frequency of 20 per mm to 100 per mm. At this point, the large-scale chevron pattern is fully segmented from the underlying surface. However, adjusting the filter cutoffs to 100 per mm to 300 per mm can further bring out the finer scale features of this pattern as shown in Figure 6C.

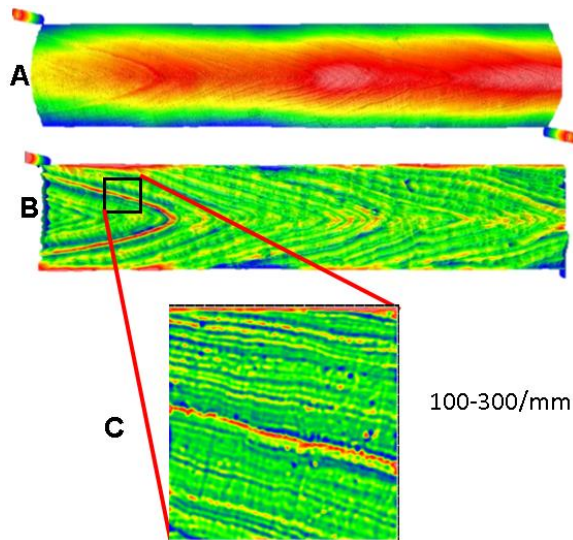


FIGURE 6. A) Unfiltered scanline. B) Scan line with cylinder removed and a Fourier bandpass filter from 20 per mm to 100 per mm. C) Filter cutoffs adjusted to 100 per mm to 300 per mm.

With chevrons isolated from the surface, areal autocorrelation was used to evaluate the angle of this heavily repeated pattern. The chevrons are measured where the scan track had reached steady state and are highly symmetric (Figure 6B). This allows for the left leaning legs of the chevron pattern (Figure 6C) to be analyzed, simplifying the analysis. ISO 25178 [14] defines three autocorrelation parameters: the fastest decay autocorrelation length (S_{al}), the texture aspect ratio (S_{tr}), and the texture direction (S_{td}). These parameters provide information not only on how directional the surface being analyzed is, but also the direction of the fastest and slowest decay of the autocorrelation length. The angle at which the major radius of the center lobe occurs gives the parameter S_{td} which coincides with the angle of the chevron pattern shown in Figure 7. Cooling length is calculated by taking half the width of the scan line divided by the tangent of the found chevron angle from the autocorrelation function.

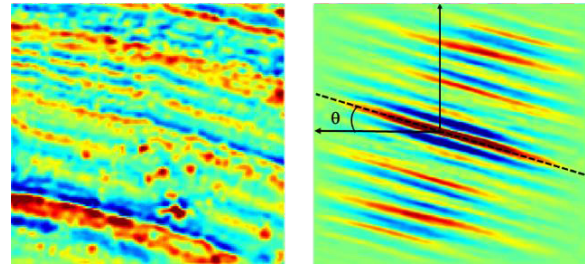


FIGURE 7. Chevron height map (Left). Autocorrelation of surface and S_{td} designated as θ (Right)

RESULTS AND DISCUSSION

From this measurement method, it is clear that the chevron pattern itself shows some variation in angle from the center of the scan line to the edges. It is likely that this is due to the legs of this pattern being slightly rounded. While this leads to some variation in angle in each scan line, this method has still proven viable in telling the differences between scan lines and approximating the cooling length of the melt pool ex situ. Figures 8 and 9 show the results from six runs of 24 scan lines and their comparison with modeling predictions for the scan track width and cooling length. Track width was measured ex-situ through microscope images taken over 1 mm of track. Images are taken at, nominally, the center of the track to avoid any edge effects. This measurement method is outlined by work conducted by Fox *et. al.* [15].

The model chosen for comparison is the Rosenthal solution [16]. The Rosenthal solution provides the analytical explanation to a moving heat source, originally developed to understand welding. Dykhuizen and Dobranich later adapted this model, applying it to laser based additive manufacturing processes [17, 18]. From Figure 8, one can see the experimental results of width measurement with error bars set to 1 standard deviation. Experimental width measurements match not only the predicted pattern, but also the approximate values modeled by the Rosenthal solution.

Cooling length measurements, shown in Figure 9 with error bars set to the largest deviation from the mean, appear to diverge from the model's predictions. This, however, was expected as the Rosenthal solution is a fairly simplified model and does not take into account some of the physical processes occurring during the build. Among those not considered is the creation of voids in the wake of the melt pool due to processing

conditions with high energy density, referred to as keyholing. Excluding the region where keyholing is expected (all power cases for the 100 mm/s and 200 mm/s cases), a linear pattern is apparent. Thought not predicted by the model, some of these linear trends have a slight negative slope. The decrease in cooling length as velocity increases for a given power is feasible as the energy imparted into the surface is decreased with faster scan speeds when all else is held constant. Results of this very slight cooling length decrease as velocity increases coincide closely with results shown by Heigel and Lane's in-situ thermographic measurements of melt pool lengths, however in both cases more results are needed [19]. Model results for cooling length could also be improved by moving toward higher fidelity finite element simulations as well as incorporating more physics into the process [20].

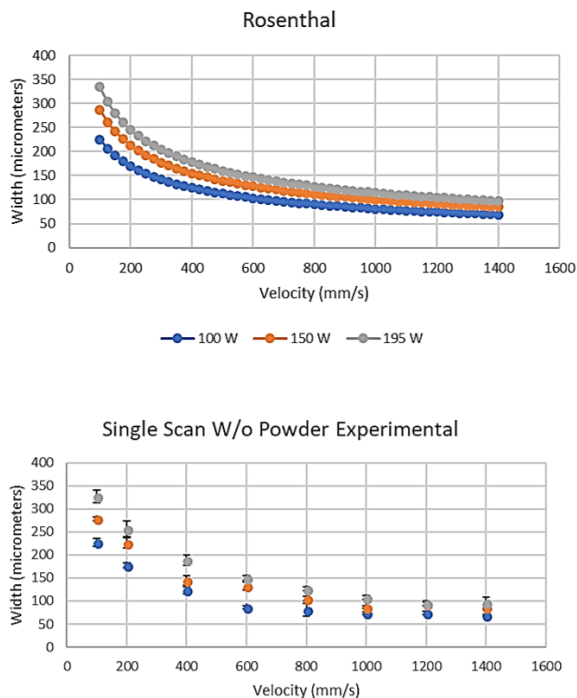


FIGURE 8. Experimental melt pool width comparison with the Rosenthal solution data (error bars set to one standard deviation).

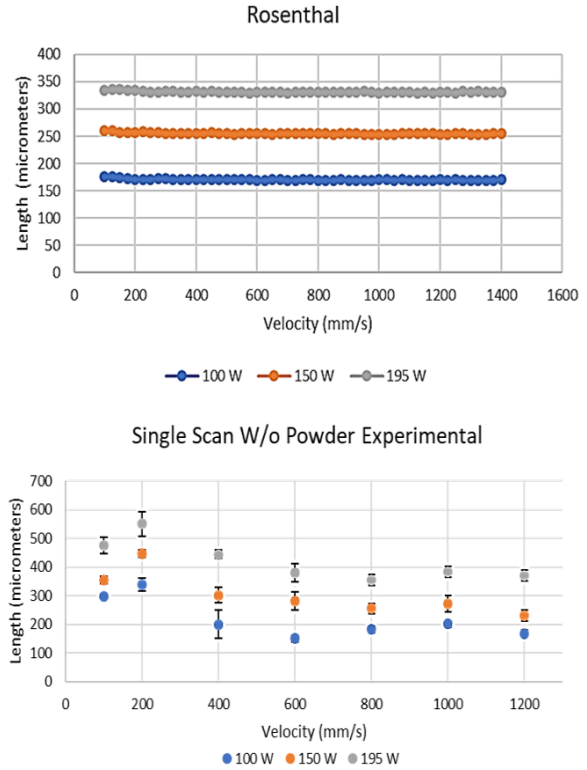


FIGURE 9. Experimental cooling length comparison with the Rosenthal solution data (error bars set to largest deviation seen).

FUTURE WORK

This work will be expanded in two major directions. The scan lines measured in this work will be sectioned and undergo microstructural analysis to relate microstructure to the length-to-depth ratio of the melt pool. This method will also be applied to single scan lines with powder as well as multiple adjacent scan tracks with and without powder to understand how this analysis method will progress when applied to building full sized parts.

REFERENCES

- [1] Mumtaz KA, Hopkinson N. Selective Laser Melting of thin wall parts using pulse shaping. *Journal of Materials Processing Technology* 2010;210:279-287. doi:10.1016/j.jmatprotec.2009.09.011
- [2] Liu X, Chu PK, Ding C. Surface modification of titanium, titanium alloys, and related materials for biomedical applications. *Materials Science and Engineering: R: Reports* 2004;47:49-121. doi:10.1016/j.mser.2004.11.001.
- [3] Lane BM, Moylan SP, Whinton EP. *PostProcess Machining of Additive*

- Manufactured Stainless Steel. Proceedings of the 2015 ASPE Spring Topical Meeting: Achieving Precision Tolerances in Additive
- [4] Yasa E, Kruth J-P, Deckers J. Manufacturing by combining Selective Laser Melting and Selective Laser Erosion/laser re-melting. *CIRP Annals - Manufacturing Technology* 2011;60:263–6. doi:10.1016/j.cirp.2011.03.063.
- [5] Measurement Science Roadmap for Metal Based Additive Manufacturing, Gaithersburg, MD: NIST; 2012.
- [6] Z. Reese *et al.* Observations on the surface morphology of laser powder bed fusion metal surfaces. *Met and Props* 2017, June 2017, Gothenburg, Sweden. Unpublished conference paper, 2017.
- [7] Fox, Jason C., Shawn P. Moylan, and Brandon M. Lane. "PRELIMINARY STUDY TOWARD SURFACE TEXTURE AS A PROCESS SIGNATURE IN LASER POWDER BED FUSION ADDITIVE MANUFACTURING." *2016 Summer Topical Meeting: Dimensional Accuracy and Surface Finish in Additive Manufacturing*. 2016.
- [8] Fox JC, Moylan SP, Lane BM. Effect of process parameters on the surface roughness of overhanging structures in laser powder bed fusion additive manufacturing. *Procedia CIRP*, Charlotte, NC: 2016. doi:10.1016/j.procir.2016.02.347
- [9] Senin, Nicola, and Richard K. Leach. "Information-rich surface metrology." *Procedia CIRP* (2018).
- [10] Gockel, Joy, and Jack Beuth. "Understanding Ti-6Al-4V microstructure control in additive manufacturing via process maps." *Solid Freeform Fabrication Proceedings*, Austin, TX, Aug (2013): 12-14.
- [11] Keller, Trevor, et al. "Application of finite element, phase-field, and calphad-based methods to additive manufacturing of Ni-based superalloys." *Acta Materialia* (2017).
- [12] Ghosh, Supriyo, et al. "On the primary spacing and microsegregation of cellular dendrites in laser deposited Ni–Nb alloys." *Modell. Simul. Mater. Sci. Eng* (2017).
- [13] Gockel, Joy, Jack Beuth, and Karen Taminger. "Integrated control of solidification microstructure and melt pool dimensions in electron beam wire feed additive manufacturing of Ti-6Al 4V." *Additive Manufacturing* 1 (2014): 119-126.
- [14] ISO 25178-2 (2012) – Surface texture: Areal - Terms, definitions, and surface texture parameters
- [15] Fox JC, Lane BM, Yeung H, "Measurement of process dynamics through coaxially aligned high speed near-infrared imaging in laser powder bed fusion additive manufacturing", *Proc. SPIE 10214, Thermosense: Thermal Infrared Applications XXXIX*, 1021407 (5 May 2017); doi: 10.1117/12.2263863
- [16] D. Rosenthal: *Trans. ASME*, 1946, vol. 68, pp. 849–66.
- [17] R. Dykhuizen and D. Dobranich: "Analytical Thermal Models for the LENS Process," Sandia National Laboratories Internal Report, 1998.
- [18] R. Dykhuizen and D. Dobranich: "Cooling Rates in the LENS Process," Sandia National Laboratories Internal Report, 1998.
- [19] Heigel, Jarred C., et al. "Measurement of the melt pool length during single scan tracks in a commercial laser powder bed fusion process." *Proc. MSEC, Los Angeles, CA* (2017): 575-591.
- [20] Francois, Marianne M., et al. "Modeling of additive manufacturing processes for metals: Challenges and opportunities." *Current Opinion in Solid State and Materials Science* 21.LA-UR-16-24513 (2017).